Key Mechanistic Features of Enantioselective C−H Bond Activation Reactions Catalyzed by [(Chiral Mono-*N*-Protected Amino Acid)−Pd(II)] Complexes

Djamaladdin G. Musaev,*,[†] Alexey Kaledin,[†] Bing-Feng Shi,[‡] and Jin-Quan Yu*,[‡]

[†]Cherry L. Emerson Center for Scientific Computation, Emory University, 1515 Dickey Drive, Atlanta, Georgia 30322, United States
[‡]Department of Chemistry, The Scripps Research Institute, 10550 North Torrey Pines Road, La Jolla, California 92037, United States

Ⓢ *Supporting Information*

ABSTRACT: Monoprotected chiral amino acids have recently been established as a class of ligand scaffolds for effecting Pd-catalyzed enantioselective C−H bond activation reactions. However, to elucidate the mechanistic details and controlling factors of these reactions, more comprehensive studies are needed. In this work we report computational investigations into the key mechanistic features of enantioselective C−H bond activation reactions catalyzed by a [chiral (mono-*N*-protected amino acid)−Pd(II)] complex. Structural analysis points to a C−H insertion intermediate in which the nitrogen atom of the ligand is bound as a neutral σ-donor. The formation of this C−H insertion intermediate could, in principle, proceed via a "direct C−H cleavage" or via "initial N−H bond cleavage followed by C−H cleavage". The computational studies presented herein show that the pathway initiated by N−H bond cleavage is more kinetically favorable. It is shown that the first step of the reaction is the N−H bond cleavage by the coordinated acetate group (OAc). In the next stage, the weakly coordinated OAc⁻ (the second acetate group) activates the *ortho*-C−H bond of the substrate and transfers the H-atom from the C-atom to the bound N-atom of the ligand. As a result, a new Pd−C bond is formed and the carbamate is converted from X-type to L-type ligand. The absolute configuration of the products that are predicted on the basis of the calculated energies of the transition states matches the experimental data. The calculated enantioselectivity is also comparable with the experimental result. On the basis of these data, the origin of the enantioselectivity can be largely attributed to steric repulsions in the transition states.
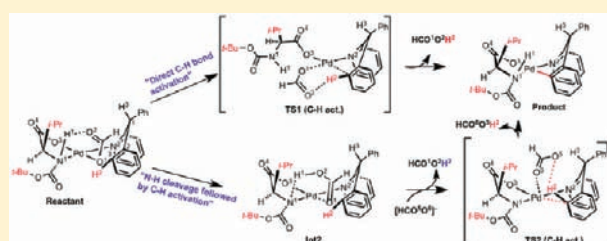
1. INTRODUCTION

Pd-catalyzed C−H bond activation reactions have been actively studied in the past decade, owing to their emerging potential for providing a diverse collection of new catalytic transformations.[1] However, in terms of reactivity, substrate scope, catalytic efficiency, chemoselectivity, and stereoselectivity, these reactions fall short of the high standard set by the most broadly used synthetic transformations, such as cross-coupling, asymmetric hydrogenation, asymmetric epoxidation, and dihydroxylation reactions. Without exception, all of these venerable transition metal-catalyzed reactions critically depend on the nature (its steric and electron properties, as well as coordination mode to the metal) of a ligand that is bound to the metal and is involved in the transition state of the key step of the catalytic cycle.[2,3] Thus, in the field of metal-catalyzed C−H functionalization, we envision that the single most important challenge is to identify a ligand that will influence the transition state energy of the C−H bond cleavage step. To pursue this goal, we first decided to use desymmetrization reactions of prochiral C−H bonds as a platform to discover chiral ligands and apply the resulting enantioselectivity values as evidence for the involvement of a ligand in the transition state of the C−H cleavage step.[4] We have recently discovered that

monoprotected amino acid ligands (MPAA) can promote Pd(II)-catalyzed enantioselective C−H activation reactions with both pyridine and carboxylic acid directing groups (see Chart 1).[5,6]

Chart 1
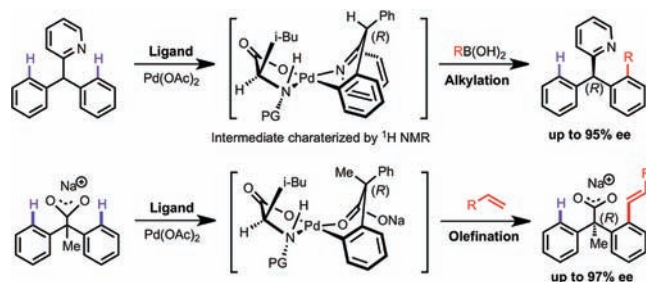
The absolute configuration of the products is consistent with a major C−H insertion intermediate that has been observed and characterized with the pyridine-containing substrate. On the basis of the absolute configuration of the product formed from

a carboxylic acid-containing substrate, we also proposed a similar C−H insertion intermediate in that closely related reaction. However, no information has been obtained on the mechanisms and important elementary steps of the reaction, the nature of the reactive species, and the transition state energies of the C−H cleavage step. We therefore decided to perform computational studies in order to gain insights into the mechanisms and important elementary steps of the reaction, the nature of the active species, the ligand coordination mode to the Pd(II), and the transition state structure of the C−H activation step. The obtained knowledge will be used to determine the origin of the observed enantioselectivity. Further understanding and development of the MPAA ligands could improve the enantioselectivity as well as regioselectivity[6] and reaction rate.[7,8]

2. COMPUTATIONAL DETAILS

Methods. All calculations were performed using the Gaussian 09 program.[9] The geometries of all reported structures were optimized without any symmetry constraint at the B3LYP level of theory in conjunction with the Lanl2dz basis set and the corresponding Hay-Wadt effective core potential (ECP) for Pd and standard 6-31G(d,p) basis sets for all remaining atoms.[10,11] This approach is subsequently referred to as B3LYP/[Lanl2dz+6-31G(d,p)].

Hessians for all structures, calculated at the B3LYP/[Lanl2dz+6-31G(d,p)] level of theory, confirmed that all reported transition states have one imaginary frequency corresponding to the reaction coordinates, and all minima have no imaginary frequency. Below, we discuss gas-phase energetics presented as $\Delta H_{gas}/\Delta G_{gas}$ using the standard harmonic approximation and the vibrational frequencies obtained by diagonalizing the mass-weighted Hessian. The Cartesian coordinates and energies of all optimized structures at the B3LYP/[Lanl2dz+6-31G(d,p)] level of theory are given in the Supporting Information.

The dielectric effects from the surrounding environment were estimated using the self-consistent reaction field IEF-PCM method[12] at the B3LYP/[Lanl2dz+6-31G(d,p)] level of theory. These corrections were made only for the most important structures. As in the experiments,[5,6] the THF was used as a solvent. Corrections to the gas phase free energies (ΔG_{gas}) due to solvent effects (ΔG_s) were estimated for the selected structures as single point IEF-PCM calculations done at the gas-phase optimized geometries: $\Delta G_{gas} + \Delta G_{solv}$. One should note that about 88−90% of PCM-contribution to energy is due to electrostatic interactions between the solute and solvent. Other components of this energy are cavitation, dispersion, and repulsion energies.

Model. In the presented calculations, the RCOO⁻ molecule was modeled by HCOO⁻. As a substrate we chose the 2-benzhydrylpyridine. Since benzoquinone (BQ) was previously shown to only improve the yield through promoting reductive elimination after the C−H activation step and has no effect on enantioselectivity,[5] we focused on the (amino acid)-Pd(II)-Sub complex using two different models as shown in Scheme 1. Model-1 is a full structure of the

Scheme 1
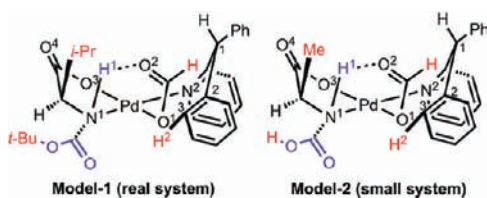
experimentally utilized[5,6] complex. In Model-2 we replaced *i*-Pr by Me and *t*Bu by H. Below, we mainly discuss the results obtained for

Model-1. Model-2 results will be discussed only in specific cases and will be explicitly stated.

3. RESULTS AND DISCUSSION

Reactants and Final Products. As could be expected, the reactant of the studied reaction is the L-Pd(II)-Sub(HCOO), **I**, complex, which has numerous isomers. Six of them are given in Figure 1. As seen from this figure, in structure **I_a** the
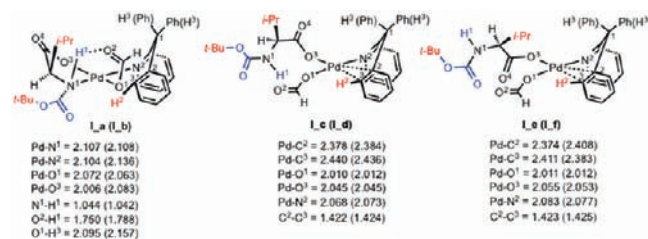

Figure 1. The calculated isomers of the reactant **I**. Isomers **I_a** and **I_b**, as well as **I_c** and **I_d**, and **I_e** and **I_f** differ from each other, respectively, by the location of the H³ and Ph ligands of the C¹-center. Ligands or numbers given without parentheses are for **I_a**, **I_c**, and **I_e**, while those given in parentheses are for **I_b**, **I_d**, and **I_f**. Distances are given in angstroms.

(HCO¹O²)⁻ ligand is coordinated to the Pd-center (by its O¹ atom) and the H¹-atom of the amino group (by its O² atom). The O¹ is also H-bonded to the H³ atom of the C¹-center. This coordination mode of (HCO¹O²)⁻ has facilitated the formation of a weak Pd−N¹ donor−acceptor bond with a 2.107 Å bond distance. Isomer **I_b** has a similar (in the **I_b** positions, H³ and Ph ligands are switched compared to those in **I_a**) bonding pattern between the (HCO¹O²)⁻, the Pd-center, and amino acid ligand L. However, in **I_b**, the O¹-center is H-bonded to the phenyl group on the C¹-center. Isomer **I_b** is found to be 9.61/9.67//9.31 kcal/mol higher in energy than **I_a** (see Table 1; here and below, the numbers given after // include solvent effects). The rotational (around the Pd−N² bond) barrier connecting **I_a** and **I_b** isomers is expected to be insignificant and was not located. Our ¹H NMR studies of the mixture of Pd(OAc)₂, substrate, and amino acid ligand are consistent with this structure (see Supporting Information).

The other four isomers of **I**, i.e. **I_c-f**, lack the N¹H¹---O²C(H)O¹ bonding pattern. In these isomers the amino acid L ligand is coordinated to the Pd-center only via its O³-atom. In isomers **I_c** and **I_d**, the second O-atom of the carboxylate group, O⁴, is located *cis* to O², while, in isomers **I_e** and **I_f**, the O⁴ and O² atoms are *trans* to each other. In **I_c-f**, the Pd−N¹ and HCO¹O²---H¹N¹ bonds do not exist; instead they have the Pd−C² and Pd−C³ bonds, with bond distances of 2.378 (2.384) and 2.440 (2.436) Å for **I_c** (**I_d**) and 2.374 (2.408) Å and 2.411 (2.383) Å for **I_e** (**I_f**). These isomers are ∼11−12 kcal/mol higher in energy than the N-agostic isomer **I_a**.

The experimentally observed product[5,6] of the aryl C−H bond activation reaction is the complex **P1** having the Pd−N¹, Pd−O³, Pd−C³, and Pd−N² bonds. Computations have revealed four different isomers of product **P1** (see Figure 2). Isomers **P1_(R)_cis** and **P1_(R)_trans** are the (R) stereo-isomers with the *i*-Pr ligand and the C¹ center located *cis* (at the same side of the N¹O³N²C³ plane) and *trans* (at the opposite sides of the N¹O³N²C³ plane) to each other, respectively. These isomers are separated by small energy barriers associated with either the inversion via the C¹-center or the ring-flip processes. Similarly, isomers **P1_(S)_cis** and **P1_(S)_trans** are

1691

dx.doi.org/10.1021/ja208661v | J. Am. Chem. Soc. 2012, 134, 1690−1698

Table 1. Relative Energies (in kcal/mol) of the Reported Structures on the "Direct C–H Bond Activation" Pathway of the Studied Reaction Calculated at the B3LYP/{Lanl2dz+ 6-31G(d,p)} Level of Theory in Gas-Phase and THF Solvent (at the PCM Level)

| structure		ΔH_{gas}	ΔG_{gas}	ΔG_s
I_a		0.00	0.00	0.00
I_b		9.61	9.67	9.31
I_c		12.27	11.00	
I_d		11.16	11.05	
I_e		11.97	11.22	
I_f		11.68	11.17	
TS1_c_(R)		21.41	22.80	
TS1_e_(R)		20.99	22.78	
TS1_d_(S)		18.59	19.74	
TS1_f_(S)		19.24	20.34	
Int1_c_(R)		−8.45	−7.78	
Int1_e_(R)		−3.06	−3.58	
Int1_d_(S)		−10.31	−8.98	
Int1_f_(S)		−4.56	−2.69	
P1				
	(R)_cis	[2.68]	[2.68]	[2.51]
	(R)_trans	[1.71]	[1.37]	[1.32]
	(S)_cis	[0.00]	[0.00]	[0.00]
	(S)_trans	[3.61]	[3.15]	[2.97]
P2				
	(R)	{2.43}	{0.71}	{0.51}
	(S)	{0.00}	{0.00}	{0.00}
P1 + HCOOH				
	(R)_trans	16.40	5.88	1.72
	(S)_cis	14.69	4.52	0.00
P2 + (L–H)				
	(R)	12.89	0.11	−8.78
	(S)	10.46	−0.60	−9.29
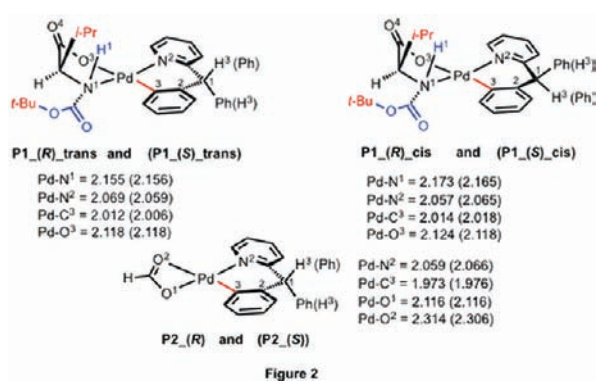
Figure 2. Calculated possible products of the Pd(II)-catalyzed C–H bond activation reaction. In the notation **Pn_(X)_z**, **Pn** stands for products **P1** and **P2**, **X** stands for stereoisomer (**R** or **S**), and **z** stands for the positioning of the *i*-Pr and C^1 chiral center (**z = cis**, if the *i*-Pr ligand and the C^1 center are located on the same side of the $N^1O^3N^2C^3$ plane; **z = trans**, if the *i*-Pr ligand and the C^1 center are located on the opposite sides of the $N^1O^3N^2C^3$ plane). Ligands or numbers given without parentheses are for (R) isomers, while those given in parentheses are for (S) isomers. Distances are given in angstroms.

the (S) stereoisomers. In these isomers the Pd–N^1, Pd–O^3, Pd–C^3, and Pd–N^2 bond distances are calculated to be within 2.155–2.173 Å, 2.118–2.124 Å, 2.006–2.018 Å, and 2.057–2.069 Å,

respectively. The energetically most stable isomer of **P1** is the (S) stereoisomer **P1_(S)_cis**. Another (S) stereoisomer, **P1_(S)_trans**, is 3.61/3.15//2.97 kcal/mol higher in energy. The (R) stereoisomers **P1_(R)_trans** and **P1_(R)_cis** are calculated to be 1.71/1.37//1.32 and 2.68/2.68//2.51 kcal/mol higher in energy than **P1_(S)_cis**.

In the course of these computational studies, we also located another possible product of the reaction, complex **P2**, where Pd is ligated by a HCOO⁻ ligand (instead of amino acid) and substrate (see Figure 2). Once again, the (S) stereoisomer of **P2_(S)** is found to be lower in energy than (R) isomer **P2_(R)** by 2.43/0.71//0.51 kcal/mol. In **P2** the calculated Pd–C^3 bond distance is slightly shorter than that in **P1**, mainly because the Pd–O^2 bond located *trans* to Pd–C^3 is extremely weak with a bond distance of 2.314 (2.306) Å.

The formation of the **P1** products, i.e. reactions

$$\mathbf{I\_a} \rightarrow \mathbf{P1\_(R)\_trans} + \text{HOOCH} \qquad (1)$$

$$\mathbf{I\_a} \rightarrow \mathbf{P1\_(S)\_cis} + \text{HOOCH} \qquad (1')$$

are calculated to be endothermic by 16.40/5.88//1.72 and 14.69/4.52//0.50 kcal/mol. Meanwhile, the energies of the reactions

$$\mathbf{I\_a} \rightarrow \mathbf{P2\_(R)} + \text{L–H} \qquad (2)$$

$$\mathbf{I\_a} \rightarrow \mathbf{P2\_(S)} + \text{L–H} \qquad (2')$$

are 12.89/0.11//−8.78 and 10.46/−0.60//−9.29 kcal/mol, respectively. In other words, the formation of experimentally reported[5,6] product **P1** (Pd complex with amino acid and substrate) is thermodynamically less favorable than that of **P2** (Pd complex with HCOO⁻ and substrate) product. As seen above, the inclusion of solvent effects make reactions 1 and 1′ only slightly endothermic, and reactions 2 and 2′ exothermic by 8.78 and 9.29 kcal/mol.

These computational findings raise two major questions: (1) Why do experiments lead to the thermodynamically less favorable (R) stereoisomer **P1_(R)_cis** rather than the energetically more favorable (S) stereoisomer **P1_(S)_cis**? (2) Why do experiments observe thermodynamically less favorable product **P1** (both (R) and (S)) rather than **P2_(S)_cis** product?

To answer these questions, we study all possible mechanisms of the C–H bond activation in complex **I** in detail. In general, reactions 1 or 1′ and 2 or 2′ could proceed via two different pathways: (a) Direct C^3–H^2 bond activation and (b) the N^1–H^1 bond cleavage and subsequent C^3–H^2 bond activation followed by the N^1–H^2 bond formation. Both pathways may proceed with or without assistance of HCOO⁻. Our preliminary studies on Model-2 show that the C–H activation on the Pd-center (without involvement of HCOO⁻) is kinetically infeasible; therefore, it will not be discussed below. This finding is consistent with the conclusions of numerous previous studies of C–H bond activation of other Pd(II) complexes.[13,14]

Direct C–H Bond Activation Pathway. For the reaction to proceed via this pathway, at first, the I_a → I_c (or I_d) or I_a → I_e (or I_f) isomerization should take place (Figure 1). As seen in Table 1, the I_a → I_c (or I_d) or I_a → I_e (or I_f) isomerization requires 12.27/11.00 (or 11.16/11.05) and 11.97/11.22 (or 11.68/11.17) kcal/mol energy, respectively. As mentioned above, we did not study barriers associated with these isomerization processes, but in any case, they are not

expected to contribute to the final mechanism and stereo-selectivity of reactions 1 and 1′ and 2 and 2′.

At the next stage, the coordinated HCOO ligand attacks the H^2-atom and activates the C^3-H^2 bond at the transition state **TS1**. This transition state is an important one and controls the formation of (R) and (S) stereoisomers. In Figure 3, we present
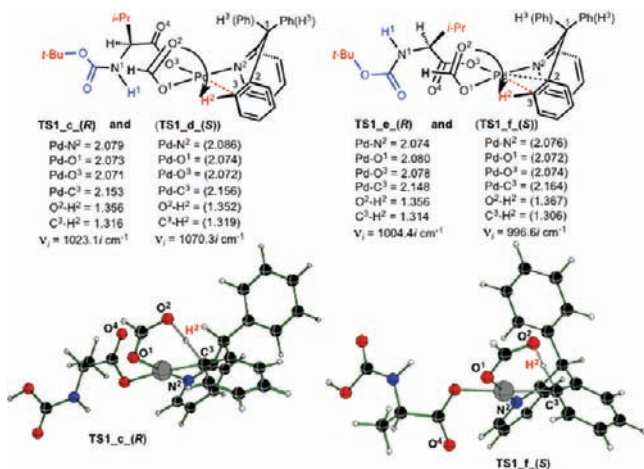

Figure 3. Calculated C−H bond activation transition state (**TS1**) of the "direct C−H bond activation" pathway. In the notation **TS1_z_(X)**, **TS1** stands for transition state, **z** stands for the connected prereaction complex, and **X** stands for stereoisomer (R or S). Ligands or numbers given without parentheses are for (R) isomers, while those given in parentheses are for (S) isomers. Distances are given in angstroms. For the sake of simplicity, here, as an example, we explicitly present the calculated structures only for **TS1_c_(R)** and **TS1_f_(S)**, but full geometries of all reported **TS1**'s are given in the Supporting Information.

four calculated isomers of this transition state: **TS1_c_(R)**, **TS1_d_(S)**, **TS1_e_(R)**, and **TS1_f_(S)** (here **c−f** stand for the prereaction complexes connected directly by this transition state, and (R) and (S) stand for the stereoisomers of the resulting intermediate, **Int1**).

The performed IRC calculations show that (a) **TS1_c_(R)** connects structure **I_c** with intermediate **Int1_c_(R)**, (b) **TS1_d_(S)** connects structure **I_d** with intermediate **Int1_d_(S)**, (c) **TS1_e_(R)** connects structure **I_e** with intermediate **Int1_e_(R)**, and (d) **TS1_f_(S)** connects structure **I_f** with intermediate **Int1_f_(S)**. The presented important geometry parameters of these transition states are consistent with their nature. As seen in Figure 3, in general, at these transition states the broken C^3-H^2 bonds are elongated to *ca.* 1.31−1.32 Å, and the formed O^2-H^2 and $Pd-C^3$ bonds are shrunk to *ca.* 1.35−1.37 Å and *ca.* 2.15−2.16 Å, respectively. Other geometry parameters of these transition states are similar to those in the corresponding prereaction complexes. The calculated normal modes with imaginary frequencies of 1023.1i, 1070.3i, 1004.4i, and 996.6i cm^{-1} are fully consistent with the nature of these transition states, too.

The energy barriers for the **I_a → Int1** rearrangement, calculated relative to **I_a**, are 21.41/22.80, 20.99/22.78//22.85, 18.59/19.74//20.19, and 19.24/20.34 kcal/mol, at the **TS1_c_(R)**, **TS1_e_(R)**, **TS1_d_(S)**, and **TS1_f_(S)**, respectively (see also the right-hand side of Figure 4). Thus, the lowest energy barriers on the potential energy surface of the "direct C−H bond activation" pathway are 20.99/22.78//22.85 and 18.59/19.74//20.19 kcal/mol at the **TS1_e_(R)** and **TS1_d_(S)**, respectively. Overcoming these energy barriers
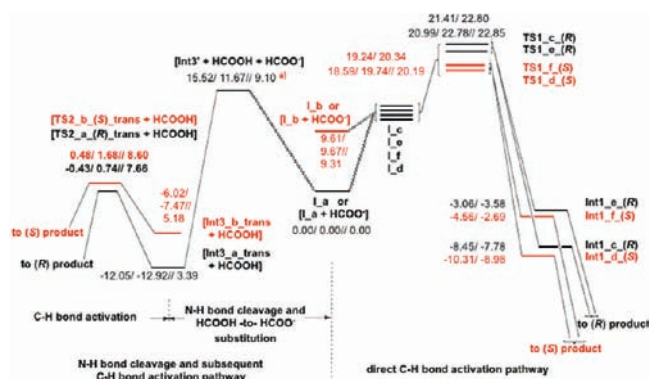

Figure 4. Schematic presentation of important mechanistic steps of the "direct C−H bond activation" (right) and "N−H bond cleavage and subsequent C−H bond activation" (left) pathways of the studied reaction. Energetics are presented as $\otimes H_{gas}/\otimes G_{gas}//[\otimes G_{solv}]$ in kcal/mol. This scheme is scaled to the $\otimes H_{gas}$ value. (a) This is the upper-limit of the energy barrier required for the HCOOO-to-HCOO$^-$ substitution.

leads to formation of the intermediates **Int1_e_(R)** and **Int1_d_(S)**, respectively. In other words, as seen in Figure 4, if the reaction would follow a "direct C−H bond activation" pathway, the formation of (R) product would be kinetically 2.40/3.04//2.66 kcal/mol *less favorable* than the formation of (S) product.

The resulting intermediates **Int1_c_(R)**, **Int1_d_(S)**, **Int1_e_(R)**, and **Int1_f_(S)** (see Figure 5) are 8.45/7.78,
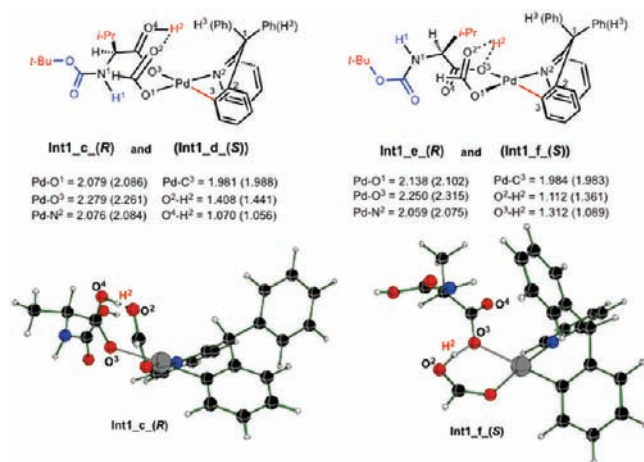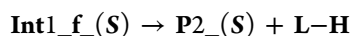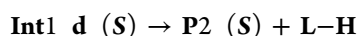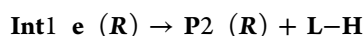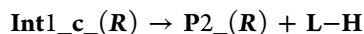

Figure 5. Calculated isomers and important geometry parameters of the intermediate **Int1** of the "direct C−H bond activation" reaction. In the notation **Int1_z_(X)**, **Int1** stands for the intermediate of the "direct C−H bond activation" reaction, **z** stands for the connected prereaction complex, and **X** stands for stereoisomer (R or S). Ligands or numbers given without parentheses are for (R) isomers, while those given in parentheses are for (S) isomers. Distances are given in angstroms. For the sake of simplicity, here, as an example, we explicitly present the calculated structures only for **Int1_c_(R)** and **Int1_f_(S)**, but full geometries of all reported **Int1**'s are give in the Supporting Information.

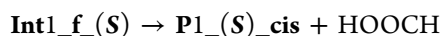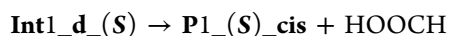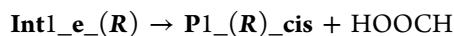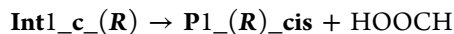10.31/8.98, 3.06/3.58, and 4.56/2.69 kcal/mol lower in energy than the energetically most favorable reactant **I_a**. As seen from Figure 5, in intermediates **Int1_c_(R)**, **Int1_d_(S)**, and **Int1_f_(S)**, the H^2 atom is transferred from HCOO^2−H^2 to the O^4 (or O^3) center of the amino acid: the calculated O^2-H^2 bond distance in **Int1_c_(R)**, **Int1_d_(S)**, and **Int1_f_(S)** is

1.408, 1.441, and 1.361 Å, respectively. In intermediates **Int1_e_(R)**, the HCOOH fragment is H-bonded to μ-oxo ligand O^3. In any case, we have found that the H-shuttling between the HCOO and the amino acid is energetically a less demanding process (not shown here).

Comparison of the Pd$-O^3$ bond in prereaction complexes (in Figure 1) **I_c-f** and the corresponding intermediates **Int1_c-f** (in Figure 5) shows that in the latter the amino acid ligand is effectively detached from the Pd-center: the Pd$-O^3$ bond distances are by 0.25−0.30 Å longer in intermediates than in corresponding prereaction complexes. Meantime, the Pd$-O^1$ bond distance is only 0.06−0.07 Å longer in **Int1_c-f** than in **I_c-f**. These geometry changes indicate that the dissociation of amino acid ligand (**L-H**, below) from the intermediates **Int1_c-f** is relatively easier than the HCOOH dissociation. The reactions

$$\text{Int}1\_c\_(R) \rightarrow \text{P2}\_(R) + \text{L}-\text{H}$$

$$\text{Int}1\_e\_(R) \rightarrow \text{P2}\_(R) + \text{L}-\text{H}$$

$$\text{Int}1\_d\_(S) \rightarrow \text{P2}\_(S) + \text{L}-\text{H}$$

$$\text{Int}1\_f\_(S) \rightarrow \text{P2}\_(S) + \text{L}-\text{H}$$

are calculated to be 21.34/7.89, 15.95/3.69, 20.77/8.38, and 15.02/2.09 kcal/mol endothermic, respectively. Meantime, the reactions

$$\text{Int}1\_c\_(R) \rightarrow \text{P1}\_(R)\_\textbf{cis} + \text{HOOCH}$$

$$\text{Int}1\_e\_(R) \rightarrow \text{P1}\_(R)\_\textbf{cis} + \text{HOOCH}$$

$$\text{Int}1\_d\_(S) \rightarrow \text{P1}\_(S)\_\textbf{cis} + \text{HOOCH}$$

$$\text{Int}1\_f\_(S) \rightarrow \text{P1}\_(S)\_\textbf{cis} + \text{HOOCH}$$

are found to be endothermic by 24.85/13.66, 19.46/9.46, 25.00/13.50, and 19.25/7.21 kcal/mol, respectively. *In other words, the formation of P2 product from Int1_c−f is more favorable than the formation of the experimentally observed product P1.*

In summary, if the C−H bond activation in complex **I_a** would proceed via the direct C−H activation pathway, then (1) the C−H bond activation would occur with 20.99/22.78// 22.85 and 18.59/19.74//20.19 kcal/mol energy barriers, leading to (R) and (S) and intermediates **Int1_e_(R)** and **Int1_d_(S)**, respectively. In other words, the formation of the (R) stereoisomer would be kinetically slightly less favorable than that of the (S) stereoisomer, and (2) the final product of the reaction would be complex **P2** [Pd(II) complex with HCOO (i.e., AcO and substrate)] rather than the experimentally reported complex **P1** [Pd(II) complex with amino acid and substrate]. However, both of these computational findings contradict the available experimental data.[5,6]

N−H Bond Cleavage and Subsequent C−H Bond Activation Pathway. For the sake of simplicity, we divide discussion of this pathway into two parts. Part-1 (see Scheme 2, where we present the process initiated exclusively from the cis "**a**" isomer) involves **I_a** reactant, the N^1-H^1 bond cleavage transition state (**TS(N−H cleav)**), HCOOH-to-HCOO⁻ substitution (**Int2-to-Int3**), and final product, intermediate **Int3**. Part-2 starts from the intermediate **Int3** and follows the C^3-H^2 bond cleavage and N^1-H^2 bond formation steps (see below).

Our exhaustive calculations (at the Model-2 level) indicate that the N^1-H^1 bond cleavage in **I_a** (and **I_b**) occurs with a ~5 kcal/mol energy barrier and leads to intermediate **Int2_a** (**Int2_b**): the reactions **I_a** → **Int2_a** and **I_b** → **Int2_b** are

Scheme 2
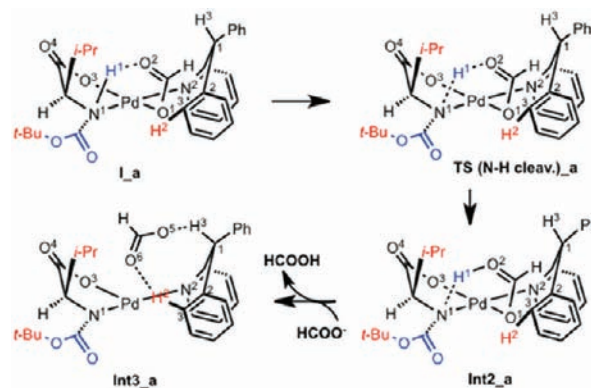
found to be endothermic by 4.13/3.74 and 5.49/5.41 kcal/mol, respectively. At the next stage, the HCOOH-to-HCOO⁻ substitution occurs, which leads to intermediate **Int3_a** (or **Int2_b**). Overall, Part-1, i.e. reactions **I_a** → **Int3_a** and/ or **I_b** → **Int3_b**, is found to be exothermic by 4.50/5.68 and/or 5.51/6.87 kcal/mol, respectively. For the real system, i.e. for Model-1, the reaction **I_a** → **Int3_a_trans** is found to be even more exothermic, 12.05/12.92 kcal/mol, in the gas-phase (see below). Inclusion of solvent effects makes it slightly (3.39 kcal/mol) endothermic (see the left-hand side drawing in Figure 4).

Although the overall reaction **I_a** → **Int3_a_trans** is exothermic (or only slightly endothermic in solution), it proceeds with a significant energy barrier. The first step of this reaction, i.e. the N^1-H^1 bond cleavage, requires only a moderate (a few kcal/mol) energy barrier, based on our Model-2 studies. At the Model-1 level of the studies, we were not able to locate any transition state associated with this step. Therefore, we may expect the HCOOH-to-HCOO⁻ substitution to occur directly from the reactant **I_a** (or **I_b**) or from the less stable intermediate **Int2_a** (or **Int2_b**). Here, we report the related energetics only from the reactant **I_a** (the process starting from the reactant **I_b** is expected to require a much larger energy barrier and, therefore, will not be discussed). The stepwise process started by dissociation of HCOOH from **I_a** (i.e., via **I_a** → **Int2** → **Int2′** + HCOOH) requires 15.52/11.67//9.10 kcal/mol. This value could serve as the upper limit to the energy barrier of the concerted HCOOH-to-HCOO⁻ substitution, which was not studied in this work.

Thus, as seen in Figure 4, even the upper limit of the energy barrier, 15.52/11.67//9.10 kcal/mol, required for the HCOOH-to-HCOO⁻ substitution from the reactant **I_a**, is significantly smaller than the 20.99/22.78//22.85 and 18.59/ 19.74//20.19 kcal/mol energy barrier found for the "direct C−H bond activation" pathway, which also starts from the same reactant. *On the basis of these data, we conclude that the first possible bond breaking event of the reactant I_a would be the N−H bond cleavage coupled with the HCOOH-to-HCOO⁻ substitution leading to Int3, rather than "direct C−H bond activation" discussed in the previous section.* The N−H bond cleavage converts the nitrogen atom to a X-type ligand and promoted the departure of the HCOO ligand. This series of events creates a vacant site for arene to coordinate, which is essential for the C−H cleavage step through a deprotonation pathway (Figure 7). Although a similar deprotonation mechanism was computed with the Pd(0)/ArI/PPh₃ catalytic system,[14] C−H cleavage by the Pd(II) catalyst presented here represents a different catalytic reaction. This mechanistic understanding offers valuable insight for

further optimization of this new amino acid with respect to the protecting group on the nitrogen.

The intermediate **Int3** is the prereaction complex for the C–H activation and has a myriad of isomers. Four of them (**Int3_a_trans, Int3_a_cis, Int3_b_trans, Int3_b_cis**) that are connected to the corresponding C^3–H^2 bond activation product **Int4** via the transition states **TS2** are given in Figure 6. One should note that the **Int3_a** and **Int3_b** isomers are direct products of the reactants **I_a** and **I_b**, respectively.

As seen from Figure 6, in all isomers of **Int3**, the HCOO fragment is H-bonded to phenyl rings and/or the H^3-atom of
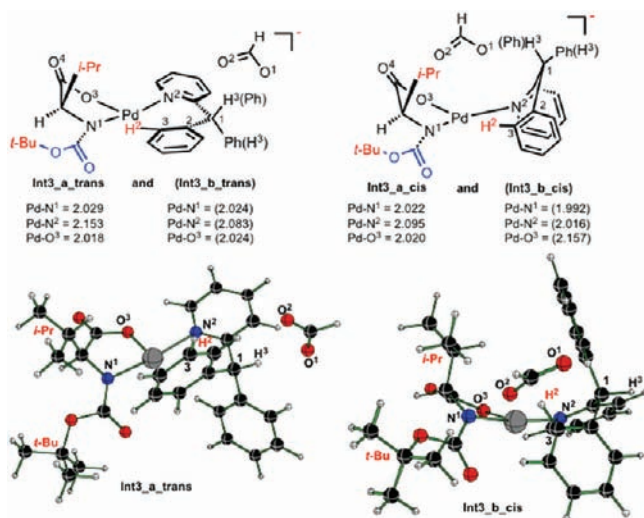

Figure 6. Calculated isomers and important geometry parameters of the intermediate **Int3** that is a result of the N–H bond cleavage followed by the HCOOH-to-HCOO⁻ substitution. In the notation **Int1_z_x**, Int3 stands for intermediate, **z** stands for the connected prereaction complex, and **x** stands for the positioning of the *i-Pr* and C^1 chiral center (**x** = **cis**, if the *i-Pr* ligand and the C^1 center are located on the same side of the $N^1O^3N^2C^3$ plane; **x** = **trans**, if the *i-Pr* ligand and the C^1 center are located on the opposite sides of the $N^1O^3N^2C^3$ plane). Distances are given in angstroms. For the sake of simplicity, here, as an example, we explicitly present the calculated structures only for **Int3_a_trans** and **Int3_b_cis**, but full geometries of all reported **Int3**'s are give in the Supporting Information.

the C^1-center. These isomers easily rearrange into each other, among which the isomer **Int3_a_trans**, where the *i-Pr* ligand and C^1-center are *trans* to each other, is calculated to be 5–7 kcal/mol more stable than other isomers (except isomer **Int3_b_cis**, which is 19.34/20.39 kcal/mol higher than **Int3_a_trans**, presumably due to strong steric repulsion between *i-Pr* and Ph ligands). Therefore, for the sake of simplicity, below we consider the energetically most favorable **Int3_a_trans** isomer as a prereaction complex for *ALL* subsequent C–H bond activation processes and report the energy barriers at the transition state **TS2** relative to this complex.

TS2 for the arene C^3–H^2 bond activation is the most intriguing structure on the potential energy surface of the "N–H bond cleavage and subsequent C–H bond activation" pathway: in fact, it controls the stereoselectivity of the reaction, i.e. the formation of (*R*) or (*S*) stereoisomers. The lowest energy barriers at the transition states **TS2_a_(R)_trans** and **TS2_b_(S)_trans** (see Figure 7; these transition states lead to the (*R*) and (*S*) stereoisomers and are connected to the **Int3_a_trans** and **Int3_b_trans** prereaction complexes, respectively) are 11.62/

13.66//11.05 and 12.53/14.60//11.99 kcal/mol, respectively. As seen in Figure 7, at the transition state **TS2_a_(R)_trans**,
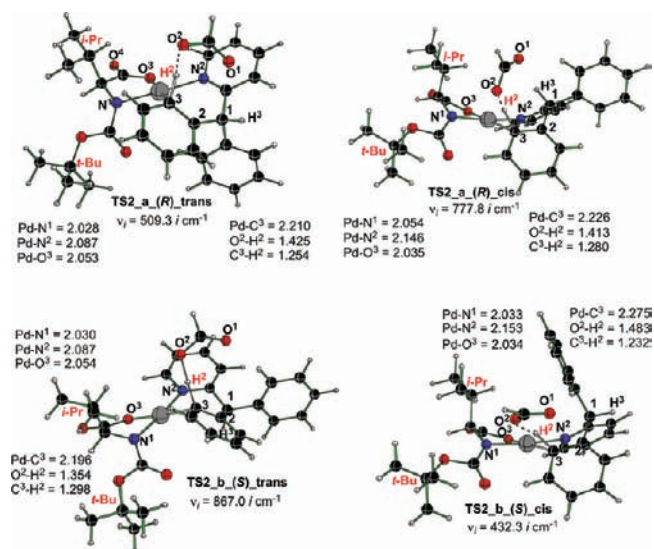

Figure 7. Calculated C–H bond activation transition states (**TS2**) of the "N–H bond cleavage and subsequent C–H bond activation" pathway. In the notation **TS2_z_(X)_y**, **TS2** stands for the intermediate, **z** stands for the connected prereaction complex, **X** stands for stereoisomer (*R* or *S*), and **y** stands for the positioning of the *i-Pr* and the C^1 chiral center (**y** = **cis**, if the *i-Pr* ligand and the C^1 center are located on the same side of the $N^1O^3N^2C^3$ plane; **y** = **trans**, if the *i-Pr* ligand and the C^1 center are located on the opposite sides of the $N^1O^3N^2C^3$ plane). Ligands or numbers given without parentheses are for (*R*) isomers, while those given in parentheses are for (*S*) isomers. Distances are given in angstroms.

the broken C^3–H^2 bond distance is elongated to 1.254 Å, and the formed Pd–C^3 and O^2–H^2 bond distances are 2.210 and 1.425 Å, respectively. Similarly, at the **TS2_b_(S)_trans** the calculated C^3–H^2, Pd–C^3, and O^2–H^2 bond distances are 1.298, 2.196, and 1.354 Å, respectively. One should note that two other studied transition states, **TS2_a_(R)_cis** and **TS2_b_(S)_cis**, where the *i-Pr* ligand and C^1-center are located *cis* to each other, lead to **Int4_(R)_cis** and **Int4_(S)_cis** isomers, respectively. However, these transition states are energetically 0.35/1.39 and 6.44/7.42 kcal/mol higher than the most favorable transition states **TS2_a_(R)_trans** and **TS2_b_(S)_trans**, respectively.

The calculated large energy difference in **TS2_b_(S)_trans** and **TS2_b_(S)_cis** can be explained by the existence of strong steric repulsion between the HCOO-fragment, on one side, and the *i-Pr* and phenyl (located on C^1-center) ligands, on the other side. As a result, **TS2_b_(S)_cis** becomes more reactant-type than **TS2_b_(S)_trans** (see Figure 7).

In summary, the above presented results show that the energy barrier for the formation of the (R) stereoisomer is (by 0.91/0.94 kcal/mol) smaller than that for the formation of the (S) stereoisomer, which would be expected to give approximately 60% ee at room temperature. Our experimental data with both pyridine and carboxylic substrates showed that *the (R) stereoisomer was the predominant product*.[5,6] The enantioselectivity obtained with the pyridine substrate and the same ligand (Boc-Valine) was 70% ee.[5] On the basis of these data, the origin of the enantioselectivity can be largely attributed to steric repulsions in the transition states **TS2**.

Transition states **TS2_a_(R)_trans**, **TS2_b_(S)_trans**, **TS2_a_(R)_cis**, and **TS2_b_(S)_cis** are confirmed to be real transition states with one imaginary frequency of 509.3i, 777.8i, 867.0i, and 432.3i cm^{-1}, respectively. Normal mode analyses show that these imaginary frequencies correspond to the C^3–H^2 bond cleavage and Pd–C^3 and O^2–H^2 bond formation. The performed IRC calculations confirm that **TS2_a_(R)_trans**, **TS2_b_(S)_trans**, **TS2_a_(R)_cis**, and **TS2_b_(S)_cis** connect prereaction complexes **Int3_a_trans**, **Int3_b_trans**, **Int3_a_cis**, and **Int3_b_cis** with intermediates **Int4_(R)_trans**, **Int4_(S)_trans**, **Int4_(R)_cis**, and **Int4_(S)_cis** (see Figure 8).

Int4_(R)_trans and (**Int4_(S)_trans**)

Pd-N^1 = 2.043
Pd-N^2 = 2.090
Pd-C^3 = 2.013
Pd-O^3 = 2.111
O^2-H^2 = 0.988
C^4-H^2 = 2.150

Pd-N^1 = 2.038
Pd-N^2 = 2.091
Pd-C^3 = 2.010
Pd-O^3 = 2.111
O^2-H^2 = 1.014
C^2-H^2 = 2.429

Int4_(R)_cis and (**Int4_(S)_cis**)

Pd-N^1 = 2.126
Pd-N^2 = 2.085
Pd-C^3 = 2.034
Pd-O^3 = 2.106
O^2-H^2 = 1.014
N^1-H^2 = 1.802

Pd-N^1 = 2.125
Pd-N^2 = 2.085
Pd-O^3 = 2.106
Pd-C^3 = 2.034
O^2-H^2 = 1.014
N^1-H^2 = 1.802
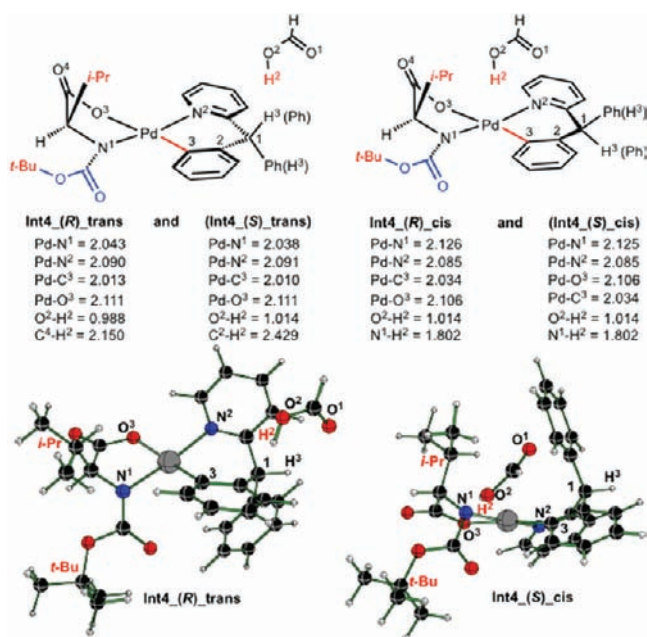
Int4_(R)_trans

Int4_(S)_cis

Figure 8. Calculated isomers and their important geometry parameters for the intermediate **Int4** that resulted after the C–H bond activation on the "N–H bond cleavage and subsequent C–H bond activation" pathway. In the notation **Int4_(X)_z**, **Int4** stands for intermediate, **X** stands for stereoisomer (R or S), and **z** stands for the positioning of the i-Pr and the C^1 chiral center (**z** = **cis**, if the i-Pr ligand and the C^1 center are located on the same side of the N^{1}O^{3}N^{2}C^3 plane; **z** = **trans**, if the i-Pr ligand and the C^1 center are located on the opposite sides of the N^{1}O^{3}N^{2}C^3 plane). Ligands or numbers given without parentheses are for (R) isomers, while those given in parentheses are for (S) isomers. Distances are given in angstroms. For the sake of simplicity, here, as an example, we explicitly present the calculated structures only for **Int4_(R)_trans** and **Int4_(S)_cis**, but full geometries of all reported **Int**'s are give in the Supporting Information.

As seen in Figure 8, at intermediates **Int4** the formation of (R) and (S) stereoisomers, that was initiated at the **TS2** structure, is completed. Intermediates **Int4_(R)_trans** and **Int4_(R)_cis** are (R) stereoisomers, which differ from each other only by the position of the i-Pr ligand and the C^1 chiral center: in **Int4_(R)_trans** they are *trans*, while in **Int4_(R)_cis** they are *cis* to each other. The isomer **Int4_(R)_trans** is 2.78/5.32 kcal/mol lower in energy than **Int4_(R)_cis**. The (S) stereoisomers, **Int4_(S)_trans** and **Int4_(S)_cis**, are 4.15/3.61 and 1.39/3.85 kcal/mol higher in energy than the most favorable (R) stereoisomer **Int4_(R)_trans**.

Thus, the overall reactions **Int3_a_trans** → **TS2_a_(R)_trans** → **Int4_(R)_trans** and **Int3_a_trans** → **TS2_b_(S)_trans** → **Int4_(S)_trans** are calculated to proceed with 11.62/13.66//11.05 and 12.53/14.60//11.99 kcal/mol barriers and

be exothermic by 7.83/7.52 and 3.68/3.91 kcal/mol, respectively. *In other words, the formation of (R) stereoisomer is more favorable than the (S) stereoisomer both kinetically and thermodynamically, which is consistent with our experimental findings.*[5,6]

At the next step, the formed HCOOH ligand in **Int4** migrates to the vicinity of the N^1-center. This occurs via either concerted or dissociation–association pathways. In any case, it is a less energy demanding process, and, therefore, will not be discussed in detail while we show its two (out of many possible), **Int4_(R)_cis_e** and **Int4_(S)_cis_f**, isomers in Figure 9.
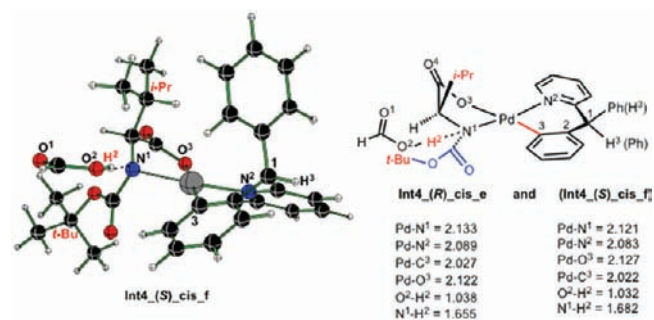

Int4_(R)_cis_e and (**Int4_(S)_cis_f**)

Pd-N^1 = 2.133
Pd-N^2 = 2.089
Pd-C^3 = 2.027
Pd-O^3 = 2.122
O^2-H^2 = 1.038
N^1-H^2 = 1.655

Pd-N^1 = 2.121
Pd-N^2 = 2.083
Pd-O^3 = 2.127
Pd-C^3 = 2.022
O^2-H^2 = 1.032
N^1-H^2 = 1.682

Int4_(S)_cis_f

Figure 9. Additional isomers of intermediate **Int4**, where HCOOH ligand is H-bonded to the N^2-center. In the notation **Int4_(X)_z_y**, **Int4**, **X**, and **z** are the same as in Figure 7, while **y** stands for the connected prereaction complex. Ligands or numbers given without parentheses are for (R) isomers, while those given in parentheses are for (S) isomers. Distances are given in angstroms. For the sake of simplicity, here, as an example, we explicitly present the calculated structures only for **Int4_(S)_cis_f**, but full geometries of all reported **Int4**'s are give in the Supporting Information.

As seen in Table 2, the **Int4_(R)_cis_e** and **Int4_(S)_cis_f** isomers are only 3.88/5.89 and 1.65/3.00 kcal/mol higher than

Table 2. Relative Energies (in kcal/mol) of All Reported Structures on the "N–H Bond Cleavage and Subsequent C–H Bond Activation Pathway" of the Studied Reaction Calculated at the B3LYP/{Lanl2dz +6-31G(d,p)} Level of Theory in Gas-Phase and THF Solvent (at the PCM Level)

structure	ΔH_{gas}	ΔG_{gas}	ΔG_s
I_a	[0.00]	[0.00]	[0.00]
Int3_a_trans + HCOOH	[−12.05]	[−12.92]	[3.39]
Int3_a_trans	0.00	0.00	0.00
Int3_b_trans	6.03	5.45	1.79)
Int3_a_cis	4.58	6.81	
Int3_b_cis	19.34	20.39	
TS2_a_(R)_trans	11.62	13.66	11.05
TS2_b_(S)_trans	12.53	14.60	11.99
TS2_a_(R)_cis	11.97	15.05	
TS2_b_(S)_cis	18.97	22.02	
Int4_(R)_trans	−7.83	−7.52	
Int4_(R)_cis	−5.05	−2.20	
Int4_(S)_trans	−3.68	−3.91	
Int4_(S)_cis	−5.64	−2.99	
Int4_(R)_cis_e	−3.95	−1.63	
Int4_(S)_cis_f	−6.18	−4.52	
Int5_(R)_trans	−2.94	−1.53	
Int5_(R)_cis	−6.60	−3.43	
Int5_(S)_trans	3.15	3.65	
Int5_(S)_cis	−6.45	−3.67	
Int5_(R)_cis_e	−2.59	−0.28	
Int5_(S)_cis_f	−5.21	−2.58	

the energetically more favorable intermediate **Int4_(R)_trans**. In intermediates **Int4_(R)_cis_e** and **Int4_(S)_cis_f**, the proton (H^2) transfer from $HCOOH^2$ to N^1-atom completes the reaction and leads to formation of the $HCOO^-$-bound intermediates **Int5** (see Figure 10). In intermediate **Int5**, the
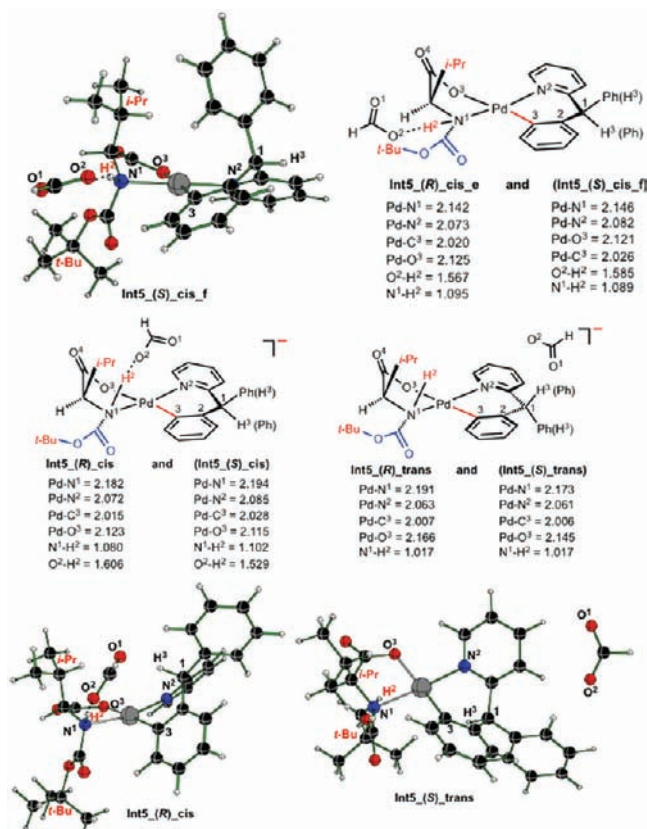

Figure 10. Calculated isomers of the intermediate **Int5** that resulted after proton transfer from HCOOH ligand to the N^2 center. For the notation **Int5_(X)_z_y**, see the caption for Figure 8. For the sake of simplicity, here, as an example, we explicitly present the calculated structures only for **Int5_(R)_cis**, **Int5_(S)_trans**, and **Int5_(S)_cis_f**, but full geometries of all reported **Int5**'s are give in the Supporting Information.

$Pd-N^1$ bond is elongated by 0.05–0.10 Å compared to the case of **Int4**, while the $Pd-N^2$, $Pd-C^3$, and $Pd-O^3$ bond distances are only insignificantly changed. The calculations show that **Int4_(R)_cis_e** → **Int5_(R)_cis_e** and **Int4_(S)_cis_f** → **Int5_(S)_cis_f** occur with less than 1.5 kcal/mol energy barrier and are only 1.36/1.35 and 0.97/1.94 endothermic, respectively. Since the existence of these transition states is not expected to contribute to the final mechanism of the overall reaction, here we did not locate the exact structures of these transition states.

As seen in Figure 10, the energetically lowest (R) isomer of **Int5** is **Int5_(R)_cis**, which is 1.55/1.23 kcal/mol lower than prereaction complex **Int4_(R)_cis**.

Dissociation of $HCOO^-$ from intermediates **Int5** leads to the final product **P1** that is reported experimentally[5,6] (Figure 2).

4. CONCLUSION

The above presented computational data and discussion show the following:

(1) The "direct arene C−H bond activation" in {[chiral mono-N-protected amino acid]−Pd(II)[2-benzhydryl-

pyridine]} complex **I_a**, in the presence of acetate (i.e., AcO), is not the operational mechanism of the (AcO)₂Pd-(II)-catalyzed enantioselective C−H bond activation reaction since it (a) proceeds with a relatively large energy barrier and (b) leads to the product distribution which is not consistent with the experimental findings.[5,6]

(2) A valid mechanism of the Pd(II)-catalyzed enantioselective C−H bond activation in **I_a** is the "N−H bond cleavage and subsequent C−H bond activation" pathway. This pathway of the reaction starts from the same reactant species and proceeds via the less energetically demanding base (OAc) assisted N−H bond cleavage step that leads to the formation intermediate with the Pd−N bond. Base-assisted C−H bond activation in this intermediate occurs with a smaller energy barrier. The calculated product distribution of the reaction via the "N−H bond cleavage and subsequent C−H bond activation" pathway [the computations show that the formation of the (R) stereoisomer is both kinetically and thermodynamically more favorable over the formation of the (S) stereoisomer] is in full agreement with the experimental findings.[5,6] On the basis of these data, the origin of enantioselectivity can be largely attributed to steric repulsions in the transition states of the newly identified reaction pathway.

(3) Preference of the "N−H bond cleavage and subsequent C−H bond activation" pathway of the reaction over its "direct C−H bond activation" pathway can be explained in terms of a greater acidity of the N−H bond over the C−H bond.

However, one should mention that the above-presented mechanistic picture is, most likely, rather simplistic. In reality, the mechanism of this reaction could be more complex and may involve several OAc fragments, which would work in a concerted (via simultaneous $Pd-O^1$ and arene C^3-H^2 bond cleavage coupled with a $Pd-C^3$ and O^6-H^2 bond formation) or a stepwise (involving the $N-H^1$ bond cleavage, C^3-H^2 bond cleavage, and $N-H^1$ bond formation steps) manner to facilitate the reaction (see Scheme 3).

Scheme 3
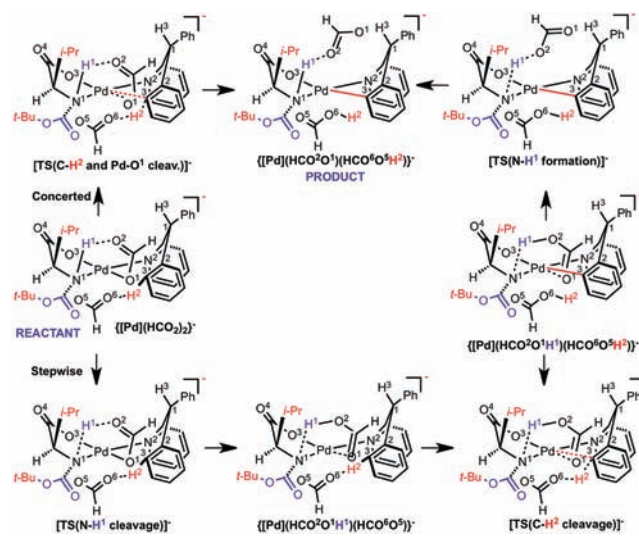
Detailed computational and experimental studies of the pathways presented in Scheme 3 are under investigation and will be reported shortly.

■ ASSOCIATED CONTENT

ⓢ Supporting Information

Complete ref 9. Stereochemical information obtained through experiments, including the following: (a) X-ray crystal data of the enantiomerically enriched (*R*) isomer of 2-((2-butyl-6-methylphenyl)(*o*-tolyl)methyl)pyridine, **2b**; (b) synthesis of the acetato-bridged dinuclear cyclopalladated complex **1b**; (c) X-ray crystal structure data for **1b**; (d) synthesis of the chloro-bridged dinuclear cyclopalladated complex **1c**; (e) X-ray crystal structure data for **1c**; (f) synthesis of the intermediates **1d** and **1e**; and (g) diastereoselective synthesis of intermediate **1d**. Computational data, including the following: (a) energies of all reported structures on the "direct C−H bond activation" pathway of the studied reaction calculated at the B3LYP/{Lanl2dz+6-31G(d,p)} level of theory in the gas-phase (Table S4); (b) energies of all reported structures on the "N−H bond cleavage and subsequent C−H bond activation pathway" of the studied reaction calculated at the B3LYP/{Lanl2dz+6-31G-(d,p)} level of theory in the gas-phase (Table S5); (c) PCM/B3LYP/{Lanl2dz+6-31G(d,p)} calculated energies (at their gas-phase optimized geometries) of the selected structures on the "direct C−H bond activation" and "N−H bond cleavage and subsequent C−H bond activation" pathways of the studied reaction [All calculations were performed in THF solvent (Table S6).]; (d) Cartesian coordinates (in Å) of all structures reported in the paper and calculated at the B3LYP/{Lanl2dz+6-31G(d,p)} level of theory (Table S7). This material is available free of charge via the Internet at http://pubs.acs.org.

■ AUTHOR INFORMATION

Corresponding Author
dmusaev@emory.edu; yu200@scripps.edu

■ ACKNOWLEDGMENTS

■ REFERENCES

(1) (a) Chen, X.; Engle, K. M.; Wang, D.-H.; Yu, J.-Q. *Angew. Chem., Int. Ed.* **2009**, *48*, 5094. (b) Daugulis, O.; Do, H.-Q.; Shabashov, D. *Acc. Chem. Res.* **2009**, *42*, 1074. (c) Lyons, T. W.; Sanford, M. S. *Chem. Rev.* **2010**, *110*, 1147.

(2) Berrisford, D. J.; Bolm, C.; Sharpless, K. B. *Angew. Chem., Int. Ed.* **1995**, *34*, 1059.

(3) Campbell, A. N.; White, P. B.; Guzei, I. A.; Stahl, S. S. *J. Am. Chem. Soc.* **2010**, *132*, 15116.

(4) For early investigations into stereochemistry in catalytic C−H activation reactions using a chiral auxiliary, see: (a) Giri, R.; Chen, X.; Yu, J.-Q. *Angew. Chem., Int. Ed.* **2005**, *44*, 2112. (b) Giri, R.; Liang, J.; Lei, J.-G.; Li, J.-J.; Wang, D.-H.; Chen, X.; Naggar, I. C.; Guo, C.; Foxman, B. M.; Yu, J.-Q. *Angew. Chem., Int. Ed.* **2005**, *44*, 7420.

(5) For the first example of Pd(II)-catalyzed enantioselective C−H activation/C−C bond formation controlled by mono-*N*-protected amino acid ligands, see: Shi, B.-F.; Maugel, N.; Zhang, Y.-H.; Yu, J.-Q. *Angew. Chem., Int. Ed.* **2008**, *47*, 4882.

(6) For Pd(II)-catalyzed enantioselective C−H activation/olefination controlled by mono-*N*-protected amino acid ligands, see: Shi, B.-F.; Zhang, Y.-H.; Lam, J. K.; Wang, D.-H.; Yu, J.-Q. *J. Am. Chem. Soc.* **2010**, *132*, 460.

(7) For ligand-controlled regioselective C−H activation, see: Wang, D.-H.; Engle, K. M.; Shi, B.-F.; Yu, J.-Q. *Science* **2010**, *327*, 315.

(8) For ligand accelerated C−H activation, see: (a) Engle, K. M.; Thuy-Boun, P. S.; Dang, M.; Yu, J.-Q. *J. Am. Chem. Soc.* **2011**, *133*, 18183. (b) Lu, Y.; Leow, D.; Wang, X.; Engle, K. M.; Yu, J.-Q. *Chem. Sci.* **2011**, *2*, 967. (c) Engle, K. M.; Wang, D.-H.; Yu, J.-Q. *J. Am. Chem. Soc.* **2010**, *132*, 14137. (d) Engle, K. M.; Wang, D.-H.; Yu, J.-Q. *Angew. Chem., Int. Ed.* **2010**, *49*, 6169. (e) Lu, Y.; Wang, D.-H.; Engle, K. M.; Yu, J.-Q. *J. Am. Chem. Soc.* **2010**, *132*, 5916.

(9) Frisch, M. J. et al. *Gaussian 09*, Revision A1; Gaussian, Inc.: Wallingford, CT, 2009.

(10) (a) Becke, A. D. *Phys. Rev. A* **1988**, *38*, 3098−3107. (b) Lee, C.; Yang, W.; Parr, R. G. *Phys. Rev. B* **1988**, *37*, 785−789. (c) Becke, A. D. *J. Chem. Phys.* **1993**, *98*, 1372−1380.

(11) (a) Hay, P. J.; Wadt, W. R. *J. Chem. Phys.* **1985**, *82*, 270−283. (b) Hay, P. J.; Wadt, W. R. *J. Chem. Phys.* **1985**, *82*, 299−310. (c) Wadt, W. R.; Hay, P. J. *J. Chem. Phys.* **1985**, *82*, 284−298.

(12) Cances, E.; Mennucci, B.; Tomasi, J. *J. Chem. Phys.* **1997**, *107*, 3032−3041.

(13) For studies concerning the mechanistic aspects C−H cleavage by Pd(II), see: (a) Ryabov, A. D.; Sakodinskaya, I. K.; Yatsimirsky, A. K. *J. Chem. Soc., Dalton Trans.* **1985**, 2629. (b) Canty, A. J.; van Koten, G. *Acc. Chem. Res.* **1995**, *28*, 406. (c) Gómez, M.; Granell, J.; Martinez, M. *Organometallics* **1997**, *16*, 2539. (d) Gómez, M.; Granell, J.; Martinez, M. *J. Chem. Soc., Dalton Trans.* **1998**, 37. (e) Biswas, B.; Sugimoto, M.; Sakaki, S. *Organometallics* **2000**, *19*, 3895. (f) Davies, D. L.; Donald, S. M. A.; Macgregor, S. A. *J. Am. Chem. Soc.* **2005**, *127*, 13754. (g) Tunge, J. A.; Foresee, L. N. *Organometallics* **2005**, *24*, 6440.

(14) For conceptually related studies concerning C−H activation with Pd(0)-PR3/Ar-X catalytic systems, see: (a) Mota, A. J.; Dedieu, A.; Bour, C.; Suffert, J. *J. Am. Chem. Soc.* **2005**, *127*, 7171. (b) García-Cuadrado, D.; Braga, A. A. C.; Maseras, F.; Echavarren, A. M. *J. Am. Chem. Soc.* **2006**, *128*, 1066. (c) Lafrance, M.; Rowley, C. N.; Woo, T. K.; Fagnou, K. *J. Am. Chem. Soc.* **2006**, *128*, 8754. (d) Pinto, A.; Neuville, L.; Retailleau, P.; Zhu, J. *Org. Lett.* **2006**, *8*, 4927. (e) García-Cuadrado, D.; de Mendoza, P.; Braga, A. A. C.; Maseras, F.; Echavarren, A. M. *J. Am. Chem. Soc.* **2007**, *129*, 6880. (f) Gorelsky, S. I.; Lapointe, D.; Fagnou, K. *J. Am. Chem. Soc.* **2008**, *130*, 10848.